ACS OMEGA

Open Access

http://pubs.acs.org/journal/acsodf

Article

Design and Numerical Simulation Study of a Novel AICD for Water Control and Gas Production in Gas Wells

Sujuan Gao, Haitao Li,* Song Nie, Ying Ai, Hongwen Luo,* and Ying Li

Cite This: *ACS Omega* 2023, 8, 39052−39066

Read Online

ACCESS | Metrics & More | Article Recommendations

ABSTRACT: The automatic inflow control device (AICD) used for water control and gas recovery in gas wells as the core component of gas well intelligent layered/segmented production and water control technology is very important for the development of advanced well completion (AWC) technology in water-producing gas reservoirs. Therefore, the design of AICD to ensure that the gas flows smoothly inside it and to keep water under control to a greater extent can maximize the performance of the AICD, and the most important thing is to restrict the water in the formation from entering the wellbore. However, currently, there are very few designs and research on the AICD used for water control and gas production in the gas wells, and the performance of this type of tool and the law of gas and water flow inside it are not perfect, so more in-depth research is needed. In this paper, a new type of AICD is designed to realize the function of water control and gas flow smoothly, and the DoE of the new AICD is carried out, determining the factors that will affect the key technical indicators and the factors that may have interactive effects, using the numerical simulation method of computational fluid dynamics to carry out optimal design, conducting fluid physical property sensitivity analysis, and flow rate applicability analysis. The results show that the tool is not sensitive to the viscosity of water and gas in different gas reservoirs but is very sensitive to the density of water and gas. When the gas/water flow rate ratio is less than 4, it can exert its water control effect. In addition, the results of multiple sets of physical experiments are well consistent with the simulation results; the average deviation of single-phase water is 10.91% and the average deviation of single-phase gas is 11.85%. Computational fluid dynamics and physical experiment results show that, under these conditions, the difference in fluid flow characteristics can be fully exploited; the channel is automatically identified to produce a small gas pressure drop and a large water flow pressure drop. The research in this paper belongs to the key technology of the AWC technology of gas wells in the new water control strategy of the current and has a certain reference value to make up for the defects of drainage gas recovery technology in the water management strategy..

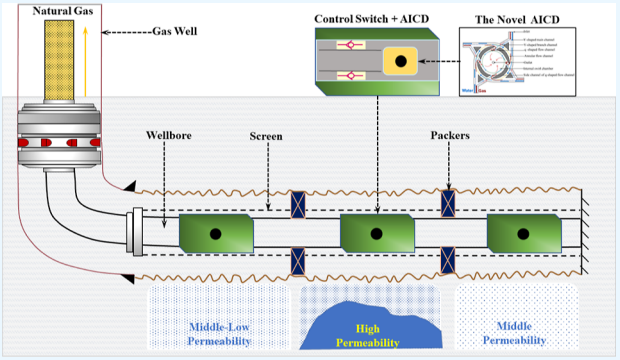

1. INTRODUCTION

As an important source of clean energy, natural gas plays an increasingly important role in today's era of global warming. Compared with petroleum and coal, its absolute combustion and remainder contents can be minimized. It is an important bridge in the process of human energy use, from the use of fossil energy with high carbon emissions after combustion, such as coal and oil, to the use of new energy sources with zero carbon emissions, such as solar energy and wind energy. Therefore, it is very important to maintain a balanced relationship between natural gas production and consumption, and increasing natural gas production is an important goal pursued by the global oil and gas industry. However, we are faced with the fact that water production is common in the development of gas reservoirs. More than half of the gas reservoirs in the world are related to aquifers.[1] A large amount of gas remains in the reservoir, resulting in a reduction in recoverable reserves, and at the same time, the recovery rate will be reduced, resulting in a reduced production of gas wells.

The root cause of water production in gas reservoirs is the water coning of gas wells. In 2002, Armenta and Wojtanowicz[2] studied on mechanisms of water coning in gas wells based on the factors of non-Darcy flow, perforation density, and the ratio of vertical-to-horizontal permeability, they found that the early water breakthrough and the large increase in water production may be the result of the combined effects of increased vertical permeability, a lower density of perforation,

Received: June 1, 2023
Accepted: September 28, 2023
Published: October 11, 2023

and high-velocity gas flow around the wells. In 2015, Feng et al.[3] proposed that water influx activity is related to the volume ratio of movable water to gas in the connected area, the contact area between gas and water, and the permeability difference between gas and water zone. In 2019, Tesha et al.[4] conducted research on water ridge control in Tertiary Sands East Africa's A1 gas field, with water cresting problems. They found that the well orientation aquifer size, height above perforation, ratio of vertical permeability to horizontal permeability (kv/kh), rate-dependent skin, and mechanical skin will all affect water production. Among them, gas reservoirs with strong reservoir heterogeneity and large interlayer differences are more prone to water channeling.[5] In addition, the water in the gas reservoir will quickly coning along the fractures in the reservoir while separating the gas area of the reservoir, it will also migrate to the area that is not invaded by water to generate "water-sealed gas", thus affecting the recoverable reserves and recovery degree of gas fields.[6] Sech et al.[7] and Qi et al.[8] found in the experimental research of water flooding gas reservoirs that the elastic production water of the gas well advances suddenly along the high-permeability formation, and the water in the low-permeability formation rises slowly; it shows that in the high-permeability zone, water is more likely to invade. From this, it can be judged that in the process of gas reservoir exploitation, strong reservoir heterogeneity, large interlayer differences, edge-bottom water coning, etc. will cause problems such as gas production profiles and uneven production degrees of each layer and, more seriously, will lead to water invasion or different degrees of water flooding. For horizontal wells, if there is a high-permeability section with strong heterogeneity in the layer that leads to local point-like water production, the productivity of the entire horizontal well will be greatly reduced even when other low-permeability sections have no water production or low water production. For vertical wells, excessively advancing water along a single layer caused by interlayer heterogeneity and edge-bottom water coning is serious, which will greatly affect the productivity of high-yield intervals or main-yield intervals and will further increase the conflict between layers, resulting in water invasion or flooding of the entire gas well.

Aiming at the abovementioned water production problem in gas reservoirs, many water control strategies are mainly adopted drainage gas recovery technology; however, the water control strategy of drainage gas recovery technology is mainly through the use of pumping units, liquid diverters, gas lifts, soap injections, flow controllers, swabbing, coiled tubing/nitrogen, venting, plunger lift, and one small concentric tubing string to reduce water accumulation in the wellbore instead of controlling water entry into the wellbore.[9] Although the drainage gas recovery technology is effective, it cannot effectively solve the impact of water coning in high-permeability layers/sections on other gas-producing layers. Once the wellbore begins to load liquid, the formation back pressure will increase and high-yield gas formations that do not produce water will also be affected, facing the risk and threat of production reduction, which in turn will affect the gas production of the entire gas well. Therefore, in the research process of water control strategies, some scholars have proposed that for unwanted water, chemical and mechanical solutions can be used to avoid unwanted water production in the wellbore design phase,[10] some scholars have proposed that delaying the water in the reservoir from entering the wellbore and controlling the water from entering the wellbore are the key to enhancing oil recovery.[9,11] Through annular flow isolation technical means such as external casing packers, swellable packers, the high-permeability section, and the low-permeability section are segmented to reduce the interaction between reservoirs,[8,12−15] Al-Khelaiwi and Davies[16] proposed for the first time the use of advanced well completions (AWCs) in water-producing gas reservoirs. The key components of AWC include downhole flow control technology such as ICD, AICD, ICV, and annular flow isolation, which can manage the fluid flow into or out of the length of the wellbore in order to optimize the well performance.[17] AWC applications using inflow control devices such as ICD/AICD/ICV and isolation technologies are needed in gas and dry gas reservoirs. However, AICD, an AWC technology in water-producing gas reservoirs, has not been described and studied in detail. Through case studies, they analyzed the application of AWCs using ICD/AICD/ICV and isolation technologies in dry gas fields, wet gas fields, and a gas-condensate field. However, as one of the key components in AWC, AICD has not been described or studied in detail.

In this paper, based on the integrated intelligent well completion technology of water detection and water control in horizontal well,[18] the gas well intelligent layered/segmented production and water control technology is proposed. The technical innovation point is that "segmentation + AICD water control + control switch" cooperates to realize layered/segmented. This technology is different from traditional drainage gas recovery technology, it closely focuses on the goal of "balanced production control" and takes "blocking large water-draining small water" as the technical concept. Using this technology to exploit horizontal wells in segments can reduce local water production section or close the water production section; to exploit vertical wells in layers, which can delay the phenomenon of water excessively advancing along a single layer or closing the high-water production layer. The gas well intelligent layered/segmented production and water control technology breaks through the shortcomings of drainage gas recovery technology in the concept of water control; this technology is more advantageous for carrying out water control in advance, and at the same time, it is more targeted in prolonging the time of water breakthrough in the wellbore, slowing down the coning of water, and improving the gas recovery. However, before the implementation of water control measures, accurate water detection is the key premise. At present, advanced and efficient water detection methods for oil and gas reservoirs can determine the fluid type and interpret the liquid production profile through the distributed temperature sensing optical fiber deviation temperature measurement technology,[19−22] to realize water detection in the water coning layer/section and the high-permeability layer/section. Among them, the automatic inflow control device (AICD) for gas wells is developed on the basis of the AICD for oil wells, which can be applied to all stages of bottom water reservoir exploitation, and AICD for gas wells can balance the liquid production profile and delay gas well water breakthrough in the stage of no water breakthrough in the gas reservoir; in the early stage of water breakthrough in the gas reservoir, it can discharge less produced water to the wellbore and play the role of drainage and gas recovery; in the middle and late stages when water production begins to increase, it can control the water production in the high-water production layer/section, balance the production profile, and improve the sweep efficiency. However, there are relatively few researches and

https://doi.org/10.1021/acsomega.3c03807
ACS Omega 2023, 8, 39052−39066

applications on AICDs for gas wells.[23] Shi et al.[24] designed an improved AICD for water control in gas wells, simulating the flow of water and gas in the AICD device field, and calculate the pressure drop of water and gas is calculated across the valve, the results show that the pressure difference of water is much greater than that of natural gas, which shows that it has a significant water-blocking effect. Zhao[25] designed a dual-entry AICD for water-producing gas wells based on the analysis of the characteristics of water−gas reservoirs and used computational fluid dynamic software to simulate different fluid flows; it can be observed that after the water enters the flow channel under the action of inertia, generally flows along the main channel, and stays inside the AICD to rotate at a higher speed, thereby inhibiting the outflow of water; when the gas flows into the device, it flows more along the radial channel. The pressure drop generated by the water passing through the AICD is much larger than that of the gas; therefore, the water-blocking effect is good. However, in the numerical simulation process of the above two AICDs used for water control in gas wells, the densities of the natural gas used are 0.55−0.90 and 0.668 kg/m^3, respectively, and the viscosities are about 0.1 and 0.1087 mPa s. In the actual gas reservoir exploitation process, the gas reservoir gas production and water control tools need to be lowered to a depth of several kilometers underground, the natural gas is in a compressed state, and the temperature, pressure, natural gas compression factor, and volume coefficient of different gas reservoirs will also be different. Zhou et al.[26] carried out the analysis of the flow characteristics of the new channel-type AICD in the bottom water−gas reservoir and the optimization of the water control completion technology, which proved that the gas recovery period with low water production in the bottom water−gas reservoirs can be extended and a better water control effect can be achieved. However, in the process of analyzing the performance of AICD, it is only described that under the same volumetric flow rate, the water−gas pressure drop ratio can reach hundreds of times, but no numerical simulation and physical experiment data are given.

The new AICD for water control and gas production in gas wells is one of the core and key components of gas well intelligent layered/segmented production and water control technology. The flow channel AICD breaks people's thinking about flow control of valve tools in the traditional sense and is a more attractive flow control tool. It has a simple structure and no moving parts and is very adaptable to harsh formation conditions. Therefore, it is very meaningful to carry out the development and design of a new AICD for water control and gas production in gas wells, but currently, there are very few designs and research on it, and the performance of this type of tool, the law of gas and water flow inside it are not perfect, so more in-depth research is needed. Based on the above problems, this paper first designs a new AICD tool based on the analysis of Y-type and q-type structural characteristics; then using the numerical simulation method of computational fluid dynamics, the structure and its geometric parameters are optimized by using 6 factors and 3 levels of orthogonal experiments and the double optimization design method considering the interaction, and determines the optimal structural parameters of the tool. Finally, this paper analyzes the sensitivity of the new AICD to different fluids and its applicability at different flow rates. In addition, the results of the multiple sets of physical experiments are highly consistent with the simulation results, indicating that the tool can effectively compensate for the defects of the drainage and gas recovery processes when applied to their completion processes of water control and gas production, and it has certain guiding significance for the accurate layered/segmented water control of the water production problem of edge and bottom water−gas reservoirs.

2. STRUCTURE AND WORKING PRINCIPLE OF THE NEW AICD

The geometric shapes of the Y-shaped flow channel, annular flow channel, and q-shaped flow channel seem simple, but the flow characteristics of fluid generated in them are very complicated, the Y-shaped/T-shaped structure can not only play the role of flow splitting and phase separation but also produce the effect of mixing, and the q-shaped structures can play the role of swirling flow. At present, these configurations have been widely used in chemical, petroleum, refining, and other industries. Hong[27] verified the two-phase flow-splitting phenomenon when air and ordinary water/variable viscosity water passed through the T-shaped joint through experiments. It is confirmed what Oranje[28] mentioned earlier is that when a part of the fluid enters the side arm, a centripetal force is generated due to an abrupt change in the direction of the gas, and an under-pressured area is created inside the 90° bend. It was also found that the reason for the difference in the split ratio was related to the gas velocity, liquid content, fluid viscosity, sidearm angle, and placement of the entire structure. Thorn et al.[29] also conducted related research on oil-gas−water three-phase measurement for the oil and gas industry. Lin[30] summarized the research on the distribution characteristics and resistance characteristics of two-phase flow in three-way pipes by multinational scholars. At the same time, it was found through experiments that whether it is a T-shaped tee pipe or a Y-shaped tee pipe or whether it is placed vertically or horizontally, there is an obvious gas−liquid phase separation phenomenon in the tee pipe; that is, there is a large difference in the dryness of the two pipes. Wang et al.[31] carried out gas−liquid two-phase flow experiments in an unequal-diameter horizontal T-junction and found that the two-phase fluid would produce phase separation in an unequal-diameter horizontal T-junction, the inertial difference of the gas−liquid two-phase fluid is the most important reason for the phase separation. Azzopardi and Rea[32] verified the phase separation characteristics of the T-junction under different conditions by installing the T-junction on the top of the oil well for field tests, through the field experimental data and a large number of literature data, together quantified under what conditions the T-joint has a good phase separation degree. In order to improve the performance of the heat exchanger, He et al.[33] conducted a phase separation study on the T-junction, which plays a role in heat exchange inside the heat exchanger, it is found that the inlet flow patterns, like slug, slug-annular, and annular flows, have a greater impact on the two-phase flow splitting of a micro-T-junction; in addition, the shape of the T-junction is circular and square, etc., which will also have a certain impact on the phase separation under different flow patterns. In order to overcome the problem of water breakthrough in oilfield horizontal wells, Zhang et al.[34] carried out a numerical study on the separation of oil and water phases by T-junction used in the AICD tool. After the separation, the AICD can increase the control of water and reduce the output of water, mainly through the three-dimensional numerical simulation of the influence of angle, fluid viscosity, flow rate,

https://doi.org/10.1021/acsomega.3c03807
ACS Omega 2023, 8, 39052−39066

etc., on the split ratio under the T-junction; it is found that the angle and viscosity have a greater impact on the split ratio of the branch, and the secondary flow and eddy current intensity generated by the branch increase with the angle. Finally, the angle range that is beneficial to oil−water separation at different viscosities is recommended. Aiming at the effects of Y-shaped and q-shaped geometry on different fluids, there have been a lot of applications and research in AICDs for oil wells, especially the fluidic diode-type AICD in the flow channel AICD is the most typical, it can guide fluid into different flow channels by means of flow channel geometry and fluid characteristics to achieve restriction of undesired fluids. Fripp et al.[35] modeled the fluid diode AICD, introduced its working principle, and compared the simulated data with the measured data through computational fluid dynamics (CFD) simulation. Additionally, single-phase laboratory testing has been documented for fluid diode AICDs in papers SPE 160165,[36] SPE167379,[37] SPE170993,[38] SPE 166285,[39] and SPE180303,[40] three case histories have been documented for fluid diode AICDs in paper SPE 166495,[41] Shahreyar et al.[42] and SPE 200255,[43] the use of fluid diode AICDs in both heavy and light oil fields were documented in the papers SPE 184094[44] and SPE 183863.[45] In addition to the above-mentioned fluid diode AICD, there are many other types of channel-type AICD, such as a new adaptable inflow control devices designed by Zeng et al.,[46,47] which guide flow through a Y-diverter and restricts water flow through a disk limiter. The automatic phase selection controller designed by Yang et al.[48] is used to suppress water production after water breakthrough in bottom water coning reservoirs; its structure looks like a q shape, which mainly depends on the difference between oil and oil viscosity; water that rotates at a high speed in the tool produces a greater pressure drop than oil that does not rotate substantially. The new AICD designed by Li et al.[49] is more suitable for horizontal wells in submerged reservoirs with high liquid production, and the automatic inflow-regulating valve (AIRV) designed by Cui et al.[50] can be used to enhance the control of water inflow before and after water breakthroughs in horizontal wells.

Natural gas as a clean energy, with its increasing consumption and the development of natural gas resources, has become a major focus of the global oil and gas industry,[20,22] the current demand for low-cost and efficient water control technology is huge, and the water control and gas production technology in gas wells with AICD as the core device is a low-cost, easy to operate, low-carbon environmental protection, and promising enhanced recovery technology to solve the current gas well water production problem. Inspired by the flow channel-type AICD in oil wells, combined with the current problems of the inhomogeneous gas reservoir and bottom water, the new AICD for water control and gas production in gas wells has a more targeted design in structure and working principle.

Figure 1 shows the new type of AICD for water control and gas production in the gas well obtained in the final optimized design. Its structural design makes full use of the principle of Y-shaped flow channel separation and phase separation, and the annular flow channel and q-shaped flow channel swirl flow theory, making water and gas depend on their own differences in physical properties, but they can also be controlled by the abovementioned basic geometric shapes to realize flow differences and flow control. The Y-shaped flow channel is tangent to the annular flow channel, and after the four Y-shaped main channels cut into the annular flow channel, it is radially penetrated by the annular flow channel. The Y-shaped branch channel is collinear with the central axis of the side channel of the q-shaped flow channel and the width is the same, and the flow channel is connected by an annular flow channel. The side channel of the q-shaped flow channel is tangent to the internal swirl chamber, and the 4 side channels of q-shaped launder channels share 1 internal swirl chamber. The blocks formed between the annular flow channels and the q-shaped flow channel isolate the fluid flowing into the annular flow channel from the fluid in the internal swirl chambers. It mainly utilizes the difference in gas and water properties to achieve path separation, aiming to fully utilize water as the continuous phase in the annular flow channel, dominated by inertial forces, and gas as the dispersed phase, dominated by viscous forces. The design and working principle of the device always focus on maximizing the restriction on water while minimizing the control of gas and increasing the valve pressure difference of water as much as possible while reducing the valve pressure difference of gas to control water and achieves the expected effect.

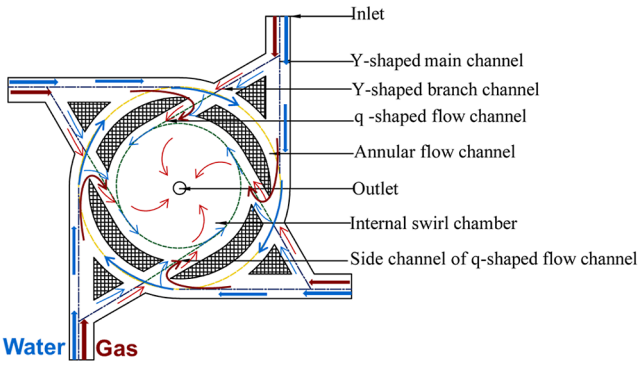

Figure 1. Structure diagram of the new AICD for water control and gas production in the gas wells.

3. OPTIMAL DESIGN

3.1. Design of Experiment and Simulation Methodology. *3.1.1. Design of Experiment.* The pressure difference between the inlet and outlet of AICD is an important index to evaluate the performance of AICD; so, in the process of structural design and optimization, the pressure drop of fluid passing through the AICD is taken as an important index. In order to describe the pressure drop relationship between gas and water more conveniently, the water−gas pressure drop ratio can also be selected as a key indicator at the same time.

Before the optimization and simulation of the new AICD, the advanced design of experiment (DoE) identifies the factors that will affect the pressure drop of the new AICD, the selected key factors and parameter ranges are shown in Table 1. The key factors, respectively, are the number of Y-shaped inlets, the angle of the Y-shaped channel, the number of q-shaped flow channels, the width of the q-shaped flow channel, the water flow rate and gas flow rate, the gas viscosity and density, and the water viscosity and density. Then, based on the orthogonal test, the structural parameters of the optimal design and the primary and secondary effects of the influencing factors are preliminarily determined. In addition, the shape optimization design of the new AICD is carried out mainly considering the interaction between the quantitative relationship between the two factors: the number of Y-shaped inlets and the number of

https://doi.org/10.1021/acsomega.3c03807
ACS Omega 2023, 8, 39052−39066

Table 1. Ranges of Key Parametric Values

parameters	ranges	units
the number of Y-shaped inlets	2−4	dimensionless
angle of the Y-shaped channel	40−60	degree
the number of q-shaped flow channels	2−6	dimensionless
width of the q-shaped flow channel	2−4	mm
water flow rate	5−15	m^3/d
gas flow rate	6−180	m^3/d
viscosity of gas	0.02−0.1	Cp
density of gas	0.8−200	kg/m^3
viscosity of water	1−1.6	cp
density of water	900−1300	kg/m^3

q-shaped launders to determine the best structural parameters. Based on the optimization of the structure, the research on the sensitivity of the physical parameters of the viscosity and density of gas and water to the new AICD was carried out to further clarify the performance characteristics of the new AICD, and finally, based on the flow rate relationship between water and gas, for example, the flow rate ratio, determines the optimum performance conditions for the new AICD.

3.1.2. Simulation Methodology. Mesh division and numerical calculation settings are illustrated by taking the final optimization result as an example. Table 2 shows the computational domain parameters and physical properties of the working fluid.

Table 2. Computing Domain Parameters and the Physical Properties of the Operating Fluid

parameter	unit	value
the number of Y-shaped inlets	dimensionless	4
angle of the Y-shaped channel	degree	60
the number of q-shaped flow channels	dimensionless	4
width of the q-shaped flow channel	mm	3
water flow rate	m^3/d	5
gas flow rate	m^3/d	60
viscosity of gas	cp	0.1
density of gas	kg/m^3	0.8
viscosity of water	cp	1
density of water	kg/m^3	998.2

3.1.2.1. Basic Governing Equations and the Turbulent Flow Model. The numerical calculation of the optimized design structure is carried out with the help of CFD software. If the liquid flowing in the new AICD is incompressible with three-dimensional unsteady turbulent flow, the fluid continuity equation and momentum equation in vector form are established in the Cartesian coordinate system as follows:

The fluid continuity equation

$$\frac{\partial \rho}{\partial t} + \nabla\cdot(\rho\vec{u}) = 0 \tag{1}$$

The momentum equation

$$\frac{D\vec{u}}{Dt} = \vec{f}_b - \frac{1}{\rho}\nabla p + \frac{\mu}{\rho}\nabla^2\vec{u} + \frac{1}{3}\frac{\mu}{\rho}\nabla(\nabla\cdot\vec{u}) \tag{2}$$

where $\frac{D\vec{u}}{Dt}$ is the inertial force term or the momentum of a fluid as a function of time; $\vec{f}b$ is the volume force; $-\frac{1}{\rho}\nabla p$ is the differential pressure; $\frac{1}{3}\frac{\mu}{\rho}\nabla(\nabla\cdot\vec{u})$ is the viscous force.

Turbulent Equation: the standard $k-\varepsilon$ model.

The choice of turbulence model relies on the physics of the flow, the level of accuracy needed, the availability of computational resources, and the time requirement for the solution.[51] The standard $k-\varepsilon$ model[52] is the most widely used turbulence model at present. It has the advantages of a wide application range and reasonable calculation accuracy. It is a turbulence calculation model for a high Re number. When encountering the problem of a curved wall flow, a strong swirl flow, and a large reverse pressure gradient, the calculation accuracy will be reduced. When the flow is incompressible and the source term is not considered, the turbulence kinetic energy, k, and its rate of dissipation, ε, are obtained from the following transport equations

$$\frac{\partial}{\partial t}(\rho k) + \frac{\partial}{\partial x_i}(\rho k u_i) = \frac{\partial}{\partial x_j}\left[\left(u + \frac{\mu_t}{\sigma_k}\right)\frac{\partial_k}{\partial x_j}\right] + G_k - G_b - \rho\varepsilon - Y_M - S_k \tag{3}$$

$$\frac{\partial}{\partial t}(\rho\varepsilon) + \frac{\partial}{\partial x_i}(\rho\varepsilon u_i) = \frac{\partial}{\partial x_j}\left[\left(u + \frac{\mu_t}{\sigma_\varepsilon}\right)\frac{\partial_\varepsilon}{\partial x_j}\right] + C_{1\varepsilon}\frac{\varepsilon}{k}(G_k - C_{3\varepsilon}G_b) - C_{2\varepsilon}\rho\frac{\varepsilon^2}{k} + S_\varepsilon \tag{4}$$

μ_t is the eddy viscosity

$$\mu_t = \rho C_\mu \frac{k^2}{\varepsilon} \tag{5}$$

G_k is the production of turbulence kinetic energy

$$G_k = -\rho\overline{u_i' u_j'}\frac{\partial \mu_j}{\partial x_i} \tag{6}$$

G_b is the generation of the turbulence effect of buoyancy

$$G_b = -\beta g_i \frac{\mu_t}{\mathrm{Pr}_t}\frac{\partial T}{\partial x_i} \tag{7}$$

$$\beta = \frac{1}{\rho}\left(\frac{\partial \rho}{\partial T}\right)_P \tag{8}$$

Y_M is the effect of compressibility

$$Y_M = 2\rho\varepsilon M_t^2 \tag{9}$$

$$M_t = \sqrt{\frac{k}{a^2}} \tag{10}$$

$$a = \sqrt{gRT} \tag{11}$$

The default values of the model constants $C_{1\varepsilon}$, $C_{2\varepsilon}$, C_μ, σ_k, and σ_ε are 1.44, 1.92, 0.09, 1.0, and 1.3, respectively.

3.1.2.2. Simulation Setup. In this study, the new AICD model is meshed by an unstructured grid-tetrahedral grid and the grid independence is verified. By setting 6 sets of grid parameters, as shown in Table 3, the pressure difference generated when the water flows through the AICD with a flow rate of 5 m^3/d is calculated, it can be seen that as the number

https://doi.org/10.1021/acsomega.3c03807
ACS Omega 2023, 8, 39052−39066

Table 3. Mesh Parameters

number	elements	pressure drop of water (Pa)	percentage changes (%)
1	100,234	37,442	
2	121,234	41,253	9.238
3	153,245	45,357	9.048
4	220,467	48,698	6.861
5	253,450	49,587	1.793
6	301,540	50,421	1.654

of elements increases, the pressure drop across the valve of water tends to rise, and when the number of grids exceeds 220,467, it gradually becomes stable, so the model with 253,450 elements is selected.

We know that the parameters and conditions suitable for the model and working conditions can improve the accuracy and reliability of the calculation results, analyze the model to a greater extent, and more realistically improve the performance of the new AICD. Therefore, when inputting parameters into the CFD model for initial conditions and boundary conditions, the velocity-inlet is selected as the inlet boundary condition, which is suitable for incompressible fluids, the outlet is set to pressure outlet, and the others are wall. In the process of single-phase gas calculation, the velocity of the input velocity-inlet is based on the gas flow rate of 60 m^3/d, the number of inlets is 4, and the area of a single inlet is 0.00002 m^2 so the velocity of a single inlet can be calculated as 8.681 m/s, combined with the gas density and viscosity shown in Table 3, according to formula 12, calculate the Reynolds number Re = 3086.4198, when Re > 2300, the flow belongs to turbulent flow

$$Re = \frac{\rho u d}{\mu} \tag{12}$$

where Re is the Reynolds number, ρ is the density, μ refers to the viscosity, u is the inlet velocity, and d is the inlet diameter.

The turbulence intensity calculated by formula 13 is I = 5.861%. In the same way, when calculating the water flow rate of 5 m^3/d under the same structure, the velocity of a single inlet is 0.723 m/s, Re = 3215.0206, which is also a turbulent flow, and I = 5.831%

$$I = 0.16Re^{-1/8} \tag{13}$$

where I is the turbulence intensity and Re is the Reynolds number.

The same method is used to set the parameters of the pressure outlet, calculate the turbulence intensity of the pressure outlet, and input the hydraulic diameter of 3 mm.

In order to better control the calculation process and improve the calculation accuracy, a finite volume technique is used to discretize the governing equations. The pressure−velocity coupling equation is solved using the SIMPLE algorithm and the momentum equations are discretized using the second-order upwind scheme. In addition, the relaxation factor is kept at the default setting and the residual of the continuity option is set as 10^{-4} and 10^{-3} for other residuals.

3.2. Orthogonal Test Design. In order to study the optimal water control performance of the new AICD for water control and gas production in gas wells, an orthogonal test was designed, and the structural parameters with the best water control effect were selected. The water−gas pressure drop ratio is used as the test index to evaluate the water control performance of the AICD; in addition, select the number of the Y-shaped inlets, the angle of the Y-shaped channel, the number of the q-shaped flow channels, and the width of the q-shaped flow channel, water flow rate, and gas flow rate as 6 test factors, which may have the greatest impact on the water−gas pressure drop ratio. Carry out an orthogonal test with 6 factors and 3 levels and simulate and optimize its structural parameters with the help of CFD software. The $L_{18}(3^7)$ orthogonal lists are shown in Table 4.

Through the calculation and analysis of the range, as shown in Table 5, and drawing the main effect diagram of each factor, as shown in Figure 2, the primary and secondary order is obtained: gas flow rate > water flow rate > angle of the Y-shaped channel > width of the q-shaped flow channel > number of the Y-shaped inlets > number of the q-shaped flow channels. Figure 2a shows the main effect diagram of water and gas flow rate, it can be seen that the biggest influence on the test index is the change of water flow rate and gas flow rate; that is, the influence is the greatest when different gas flow rate, which shows that when the water flow rate value is fixed, the water−gas pressure drop ratio will be greatly influenced when the gas flow rate is changed, and the gas flow rate and the water−gas pressure drop ratio are negatively correlated; through the range analysis and the main effect diagram of the structural parameters as shown in Figure 2b, it can be seen that, compared with the impact of the gas and water flow rate on the test indicators, the impact of the structural parameters on the water−gas pressure drop ratio is small, but there are still differences between the 4 structural parameters, there is still a certain influence on the water−gas pressure drop ratio, and there is an optimal value. Through the 18 sets of experimental results of the orthogonal test, the combination with the largest water−gas pressure drop ratio is the number of Y-shaped inlets is 2, the angle of Y-shaped channel is 60, the number of q-shaped flow channels is 4, the width of the q-shaped flow channel is 3, the water flow rate is 5 m^3/d, and the gas flow rate is 60 m^3/d.

3.3. Shape Optimization. *3.3.1. Geometric Shape Optimization.* The orthogonal test can disperse the test points evenly in the process of preliminary optimization and can select representative test points, which is an efficient and concise optimization design method, but the certain combination of levels selected in the orthogonal test is limited; the preferred results will not exceed the range of the selected levels. Although the results of the above orthogonal test and range calculation confirmed that the water flow rate and gas flow rate as test factors have a greater impact on the water−gas

Table 4. $L_{18}(3^7)$ Orthogonal List

levels	Number of Y-shaped inlets	B angle of the Y-shaped channel/°	C number of the q-shaped flow channel	D width of q-shaped flow channel/mm	E water flow rate /(m^3/d)	F gas flow rate/(m^3/d)
1	2	40	2	2	5	60
2	3	45	4	3	10	120
3	4	60	6	4	15	180

https://doi.org/10.1021/acsomega.3c03807
ACS Omega 2023, 8, 39052−39066

Table 5. Orthogonal List

	number of Y-shaped inlets	angle of the Y-shaped channel (deg)	number of the q-shaped flow channel	width of q-shaped flow channel/mm	water flow rate/(m^3/d)	gas flow rate/(m^3/d)	water−gas pressure drop ratio
1	2	40	2	2	5	65	9.513
2	2	45	4	3	10	130	3.469
3	2	60	6	4	15	195	1.991
4	3	40	2	3	10	195	2.144
5	3	45	4	4	15	65	7.519
6	3	60	6	2	5	130	4.201
7	4	40	4	2	15	130	3.777
8	4	45	6	3	5	195	2.053
9	4	60	2	4	10	65	7.856
10	2	40	6	4	10	130	3.291
11	2	45	2	2	15	195	2.044
12	2	60	4	3	5	65	10.762
13	3	40	4	4	5	195	2.068
14	3	45	6	2	10	65	8.291
15	3	60	2	3	15	130	3.889
16	4	40	6	3	15	65	7.897
17	4	45	2	4	5	130	4.052
18	4	60	4	2	10	195	2.168
k_1	5.178	4.782	4.916	4.999	5.442	8.640	
k_2	4.685	4.571	4.961	5.036	4.536	3.780	
k_3	4.634	5.145	4.621	4.463	4.519	2.078	
R	0.544	0.574	0.340	0.573	0.923	6.562	
significance of factors	gas flow rate > water flow rate > angle of Y-shaped channel > width of q-shaped flow channel > number of Y-shaped inlets > number of q-shaped flow channels						

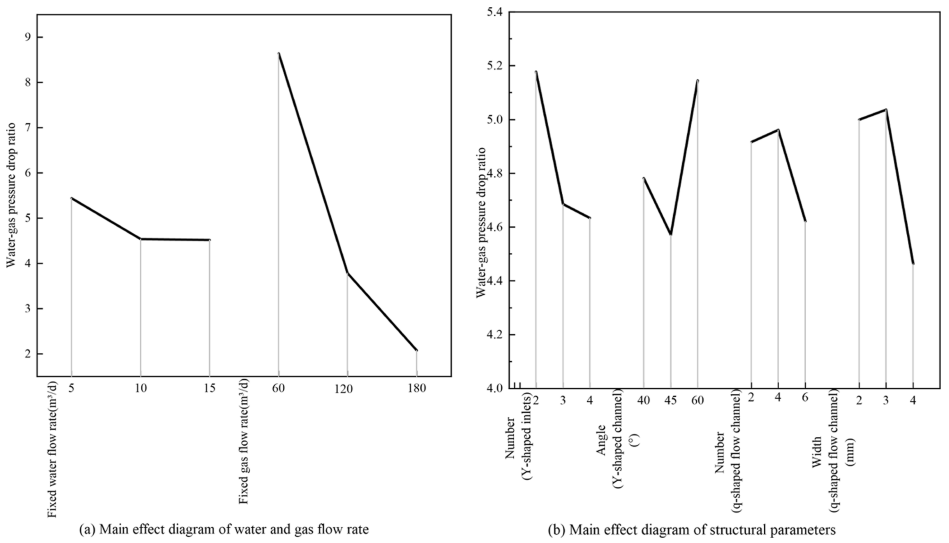

(a) Main effect diagram of water and gas flow rate

(b) Main effect diagram of structural parameters

Figure 2. Main effect diagram of orthogonal test factors.

pressure drop ratio than the structural parameters on the water−gas pressure drop ratio cannot be ignored. In order to further analyze the influence of the possible interaction between the structural parameters on the test indicators, the analysis of the interaction between the number of Y-shaped inlets and the number of q-shaped flow channels is carried out on the basis of the results obtained from the orthogonal test, mainly by expanding the value range of the two factors, and when the Y-shaped structure is used as the inlet for phase separation and flow splitting, it also needs to be combined with the q-shaped flow channel structure to provide a fast path for the gas and ensure sufficient swirl flow for the water. Therefore, the number of Y-shaped and the number of flow channels are optimized to a multiple relationship, and at the same time, it is ensured that the q-shaped flow channels do not penetrate the baffle so the number of them is limited to no more than 9. Finally, the multiple relationship between the number of Y-shaped inlets and the number of q-shaped flow channels is set as single, double, triple, and quadruple. Table 6 shows the combination scheme of the relationship between the number and multiples, a total of 17 combination schemes are obtained when the relationship between the number of Y-shaped inlets and the number of q-shaped flow channels are four kinds of multiples, and the optimization results are shown in Figure 3, which shows the 17 combination schemes under four kinds of multiples and the relationship diagram of water,

https://doi.org/10.1021/acsomega.3c03807
ACS Omega 2023, 8, 39052−39066

Table 6. Combination Scheme of the Relationship between the Number and Multiples

multiples	Single	double	triple	quadruple
the number of Y-shaped inlets	1, 2, 3, 4	1, 2, 3, 4, 2, 4	1, 2, 3, 3	1, 2, 4
the number of q-shaped flow channels	1, 2, 3, 4	2, 4, 6, 8, 1, 2	3, 6, 9, 1	4, 8, 1

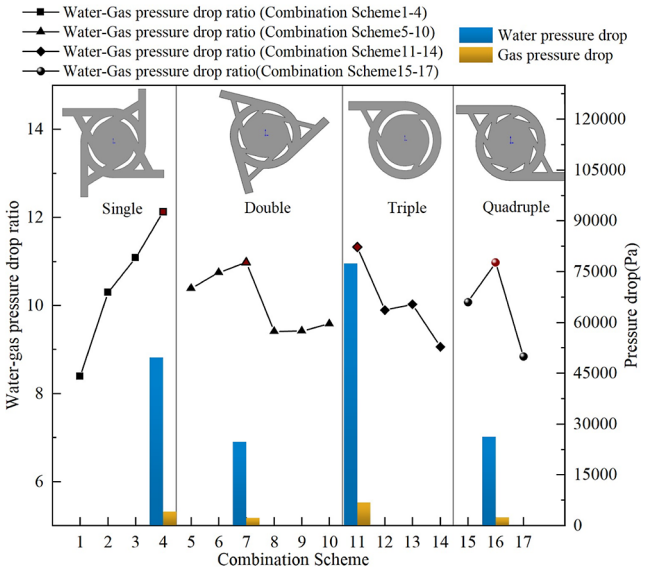

Figure 3. 17 combination schemes under four kinds of multiples and the relationship diagram of water, gas pressure drop, and water−gas pressure drop ratio in the optimal combination scheme.

gas pressure drop, and water−gas pressure drop ratio in the optimal combination scheme.

Figure 3 is the 17 combination schemes under four kinds of multiples and the relationship diagram of water, gas pressure drop, and water−gas pressure drop ratio in the optimal combination scheme, among them, when the multiple relationship between the number of Y-shaped inlets and the number of q-shaped flow channels is single, double, triple, and quadruple, the combinations are, respectively, set as combination scheme 1−4, combination scheme 5−10, combination scheme 11−14, and combination scheme 15−17. It can be seen that among the 17 combination schemes, the maximum water−gas pressure drop ratio is combination scheme 4 (4 Y-shaped inlets +4 q-shaped flow channels) when the multiple relationship is single, the maximum water−gas pressure drop ratio is combination scheme 7 (3 Y-shaped inlets +6 q-shaped flow channels) when the multiple relationship double, the maximum water−gas pressure drop ratio is the combination scheme 11 (1 Y-shaped inlet +3 q-shaped flow channels combinations) when the multiple relationship is triple, and the maximum water−gas pressure drop ratio is the combination scheme 16 (2 Y-shaped inlets +8 q-shaped flow channels) when the multiple relationship is quadruple, the figure corresponds to the models of combination scheme 4, 7, 11, and 16 and each the water pressure drop and gas pressure drop of them, the corresponding water−gas pressure drop ratios are 12.13, 10.98, 11.33, and 10.97, respectively. It can be judged that the optimal result is the combination scheme 4:4 Y-shaped inlets +4 q-shaped flow channels, which have the best water control performance.

3.3.2. Flow Law Analysis. We carry out flow law research on gas and water two-phase fluids in combination schemes 4, 7, 11, and 16, in the process of numerical simulation, continue to use the fluid physical parameters selected in the design process, and set the water volume at 5 m^3/d and the gas volume at 60 m^3/d. Figure 4 shows the water and gas pressure contour diagram and velocity streamline diagram.

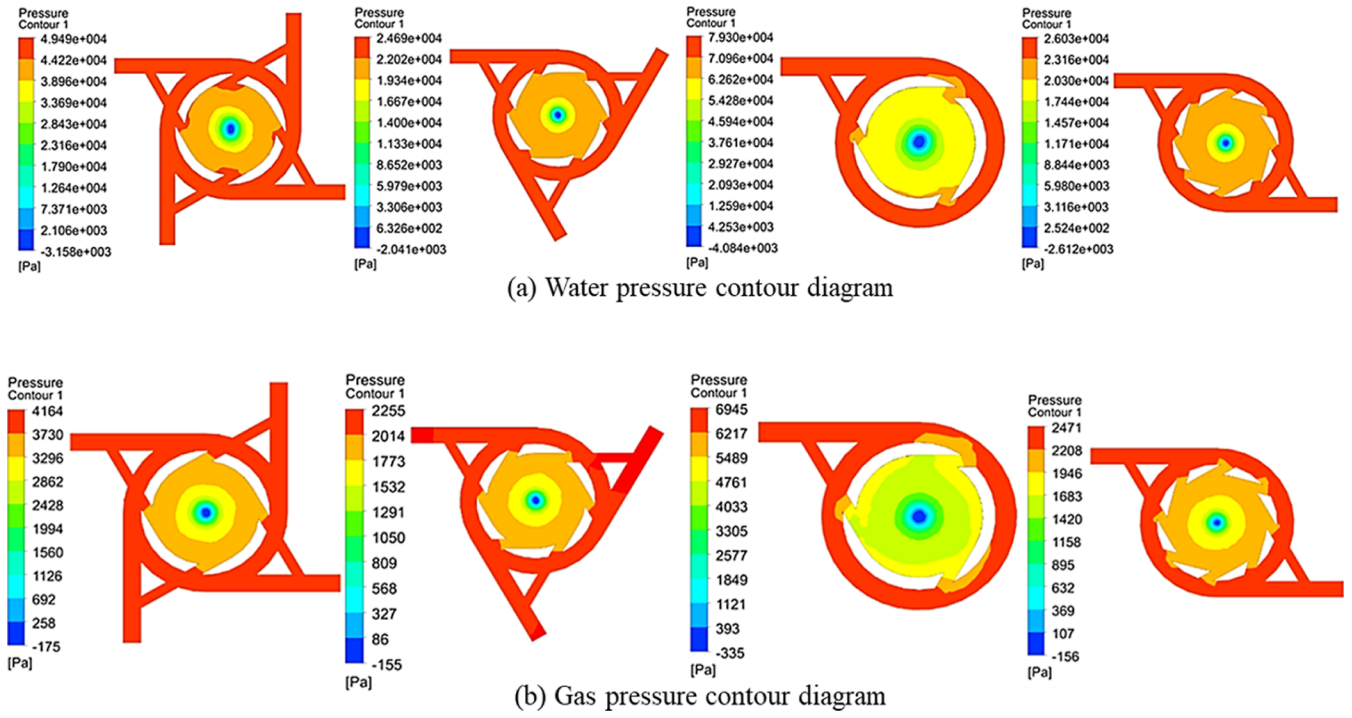

Figure 4. Water and gas pressure contour diagram.

https://doi.org/10.1021/acsomega.3c03807
ACS Omega 2023, 8, 39052−39066

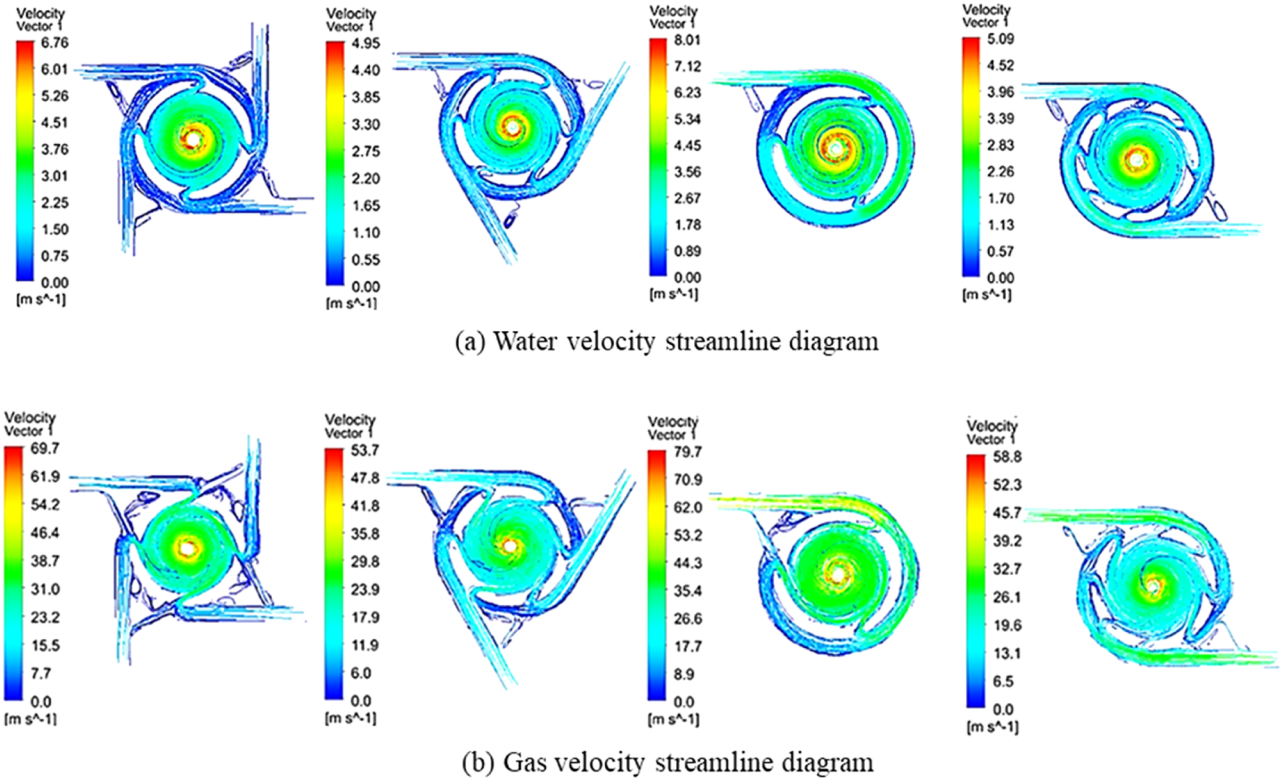

Figure 5. Water and gas velocity streamline diagram.

Figures 4 and 5, respectively, show gas and water pressure contour diagrams and velocity streamline diagrams of the best four combination schemes 4, 7, 11, and 16 under the multiple relationship between the number of Y-shaped inlets and the number of q-shaped flow channels is 1−4 times at the water flow rate is 5 m^3/d and the gas flow rate is 60 m^3/d. From the water and the gas pressure contour diagram, as shown in Figure 4a,b, it can be seen that no matter which combination, the pressure loss generated when the water passes through the tool is mainly in the internal swirl chamber and near the outlet, and the closer it is to the outlet, the greater the pressure drop gradient, and the pressure loss of the gas is mainly at the internal swirl chamber and near the outlet. The difference is that from the pressure value, the water−gas pressure drop difference is the largest when the multiple relationship is single (combination 4), followed by the multiple relationship of triple (combination 11), and the water pressure drop is the second when the multiple relationship is double and quadruple (combination 7 and 16), the gas or water pressure drop is basically the same. Observing the pressure gradient of the inner swirl chamber, it can be seen that the more the number of q-shaped flow channels, the pressure gradient of the internal swirl chamber is concentrated at the outlet, and the combination 11 is a single inlet and 3 q-shaped flow channels, it can be seen that the pressure gradient changes more, and the inlet pressure values of water and gas are at their maximum value, which is due to the pressure drop are also generated at the transition between the annular flow channel and the q-shaped flow channel. From the gas and the water velocity streamline diagram, as shown in Figure 5a,b, it can be observed that when the water enters the Y-shaped structure from the inlet, it mainly flows in along the main channel, and a small amount flows in along the branch channel, where obvious eddies can be seen. The fluid flowing in along the main channel will be divided into two parts, one part will continue to advance along the annular flow channel after merging with the downstream Y-shaped channel fluid observed in the clockwise direction under the action of inertia, and the other part will move closer to the q-shaped flow channel connected to the downstream Y-shaped branch channel observed in the clockwise direction enters the internal swirl chamber tangentially and continues to swirl until it flows out from the outlet; when the gas enters the Y-shaped structure from the inlet, it mainly flows in along the main channel, and a small amount flows in along the branch channel, but there will be no obvious eddies at the branch channel. The q-shaped flow channel connected to the branch channel of the downstream Y-shaped flow channel enters the internal swirl chamber tangentially, and continues to swirl until it flows out from the outlet; in addition, the number swirl circle of the gas in the internal swirl chamber can also be observed is significantly less than that of water. The reasons why combination 4 produced the largest water−gas pressure drop ratio, combined with the analysis of the gas and water velocity streamline diagram in Figure 5a,b, is that the water swirl flow in combination 4 is basically the same as that in combinations 7, 11, and 16, but in the case of combination 4, after the gas flows in along the Y-shaped channel, it basically enters the internal swirl chamber directly along the nearest q-shaped flow channel and basically does not flow along the annular flow channel, so the pressure drop generated by the combination 4 will be smaller, so the water control performance is the best among the four combinations.

4. RESULTS AND DISCUSSION

4.1. Fluid Sensitivity Analysis. In order to study the applicability of the new AICD when the fluid is in different

https://doi.org/10.1021/acsomega.3c03807
ACS Omega 2023, 8, 39052−39066

well conditions or different oil and gas reservoir flows in it, the research scope of viscosity and density values of gas and water is expanded. The density of natural gas is affected by temperature, pressure, and natural gas composition, the relative density of natural gas under standard conditions is between 0.55 and 0.62, and the density is 0.7174−0.8 kg/m^3 (natural gas is lighter than air). Natural gas is compressible, but due to the natural gas being exploited in different oil and gas reservoirs, the temperature and pressure of the gas reservoir are different, the compression factor and volume coefficient of natural gas will also be different so that the compression state in the formation is different, and when there are heavy components in the components of some natural gas, their relative density will be greater than 1. Combined with the temperature and pressure of the specific gas reservoir and the volume occupied by the same amount of natural gas under standard conditions, the density of natural gas in the formation can be obtained according to the compression state equation, and the density can reach 400 kg/m^3 or even greater.

The formation water density is affected by the change of mineralization, formation temperature, formation pressure, formation salinity, gas−water ratio, and salt-to-water mass ratio.[53] Schowalter[54] gave a nomograph to determine the formation water density under subsurface conditions, the formation water density range is generally 1000−1250 kg/m^3,[55] but some oil and gas reservoirs also have a formation water density in addition to the above range; therefore, the formation water density range of 900−1300 kg/m^3 was selected to study the viscosity and density sensitivity of gas and water during motion in the new AICD. Table 7 shows the parameter values of fluids under different well conditions or reservoir conditions.

Table 7. Fluid Physical Parameters for Sensitivity Analysis

fluid	parameters					
gas	density (kg/m^3)	0.8	1.25	50	100	200
	viscosity (cp)	0.02	0.04	0.06	0.08	0.1
water	density (kg/m^3)	900	1000	1100	1200	1300
	viscosity (cp)	1	1.2	1.4	1.5	1.6

Under the premise that gas and water have the same flow rate of 10 m^3/d, the numerical simulation of the flow of gas and water through the new AICD at different viscosities and densities is carried out, and the sensitivity analysis of the new AICD to gas and water viscosity and density is obtained, as shown in Figure 6. The viscosity ratio shown in Figure 6 refers to the ratio of the larger viscosity value to the minimum viscosity value. Although the viscosity values range shown in Table 7 cannot cover the viscosity values of all formations of natural gas and water, through analysis of the ratio within a certain range, the relationship between the change of the viscosity range value of natural gas and water and the change of the pressure drop value can be better observed, and the viscosity sensitivity characteristics of the new AICD can be clearly understood. Similarly, the density ratio refers to the ratio of the larger density values to the minimum density values. In addition to analyzing the density sensitivity characteristics of the new AICD, the sensitivity of AICD to viscosity and density can be analyzed within the specific flow rate and make better use of this feature of the tool.

Figure 6a shows the viscosity sensitivity analysis, it can be seen that the gas's viscosity is smaller than the viscosity of water, and the viscosity range is relatively small, but from the viscosity ratio in the figure, it can be seen that the maximum viscosity of the selected gas is 5 times the minimum viscosity of the gas, and the maximum viscosity of water is 1.6 times the minimum viscosity of water. From the pressure drop of the valve, under the same flow rate, the overall pressure drop caused by water is larger than the pressure drop caused by gas, and the pressure drop produced by both gas and water tends to decrease with the increase of viscosity, but the variation trends are all small, the difference between the pressure drop corresponding to the maximum value of the gas viscosity and the pressure drop corresponding to the minimum value of the gas viscosity is about 6 KPa, the difference between the pressure drop corresponding to the maximum value of water viscosity and the pressure drop corresponding to the minimum value of water viscosity is about 15 KPa. The above analysis can be judged: if the tool is installed in the oil and gas reservoirs with higher gas viscosity, or if the tool is installed in the oil and gas reservoir with lower water viscosity, the water control effect will be improved in the above two types of reservoirs, but the overall improvement effect is not significant.

Figure 6b shows the density sensitivity analysis, the density of gas is smaller than the density of water, and the range of gas density values is small, but the range of variation is large, while water is the opposite. From the density ratio in the figure, the maximum density of the selected gas is 250 times the minimum density of the gas and the maximum density of water is only 1.444 times the minimum density of water. From the pressure drop of the valve, under the same flow rate, the overall pressure drop caused by water is larger than the pressure drop caused by gas, and the pressure drop generated by gas and water tends to increase with the increase of density, but the pressure drop of water through the AICD is linear with the change of water density, the pressure drop of gas through the AICD is more nonlinear with the change of gas density, the change trend is relatively larger with the increase of gas density, the difference between the pressure drop corresponding to the maximum value of the gas density and the pressure drop corresponding to the minimum value of the gas density is about 47 KPa, and the difference between the pressure drop corresponding to the maximum value of water density and the pressure drop corresponding to the minimum value of water density is about 94 KPa. The above analysis can be judged: if the tool is installed in the oil and gas reservoir with a smaller gas density or the tool is installed in the oil and gas reservoir with a higher water density, the water control effect will be improved in the above two types of reservoirs, and the improvement effect is relatively good.

4.2. Flow Application Range Analysis. According to the results of the orthogonal test, it is known that the flow rate of water and gas is the main influencing factor in the design process of the new AICD structure. In order to further clarify the performance of the new AICD for gas well water control and gas production, understand the tool in the formation environment, and demonstrate its practical application value for the applicable range of water and gas flow rates, natural gas with a viscosity of 0.06 cP and a density of 50 kg/m^3, and water with a viscosity of 1 cP and a density of 998.2 kg/m^3 are selected to analyze the application range of flow rate.

Figure 7a shows the changing trend of the water−gas pressure drop ratio when the gas−water flow rate ratio is in the range of 1−4 under the premise of the fixed water flow rate of 5, 10, 15, and 20 m^3/d, and the change range of gas flow rate to

https://doi.org/10.1021/acsomega.3c03807
ACS Omega 2023, 8, 39052−39066

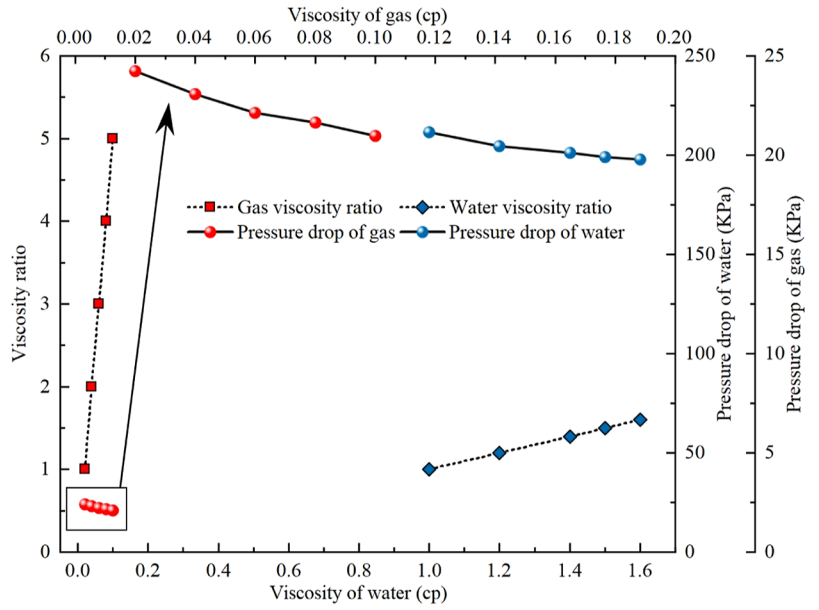

(a) Variation trend diagram of gas and water viscosity and pressure drop

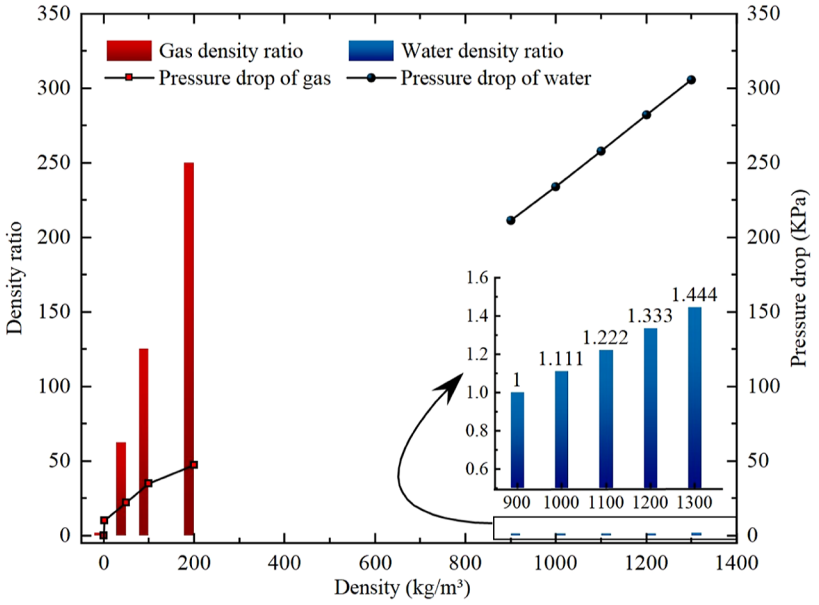

(b) Variation trend diagram of gas and water density and pressure drop

Figure 6. Fluid sensitivity analysis diagram.

achieve the water control effect of a water−gas pressure drop ratio of 1−20. No matter which fixed water flow rate value (5, 10, 15, or 20 m^3/d) is selected, the four water−gas pressure drop ratio curves almost all overlap, and all show a decreasing trend with the increase of the gas−water flow ratio, that is, the larger the gas flow rate, the smaller the water−gas pressure drop ratio. To achieve the same water−gas pressure drop ratio effect, the larger the fixed water flow rate value, the larger the gas flow range applicable to the tool. When the water flow rate is set at 5 m^3/d, the gas flow rate is in the range of 5−20 m^3/d; with the increase of the water flow rate, when the water flow rate is set at 20 m^3/d, the gas flow rate increases to the range of 25−80 m^3/d. It can be concluded that when the water−gas pressure drop ratio is about 1, the gas−water flow rate ratio reaches its maximum, which is about 4; that is, the application range of the new AICD flow rate is when the gas−water flow rate ratio is less than 4.

Figure 7b shows the changing trend of the water−gas pressure drop ratio when the gas−water flow rate ratio is in the range of 1−4 under the premise of the fixed gas flow rate value of 20, 30, 40, and 50 m^3/d, and the change range of water flow rate to achieve the water control effect of a water−gas pressure drop ratio of 1−20. No matter which fixed gas flow rate value (20, 30, 40, or 50 m^3/d) is selected, the four water−gas pressure drop ratio curves almost all overlap, and all show a decreasing trend with the increase of the gas−water flow rate ratio, the greater the water flow rate, the greater the water−gas pressure drop ratio. To achieve the same water−gas pressure drop ratio effect, the larger the fixed gas flow rate value, the larger the water flow range that the tool can adapt to. When the gas flow rate is set at 20 m^3/d, the water flow rate is in the

https://doi.org/10.1021/acsomega.3c03807
ACS Omega 2023, 8, 39052−39066

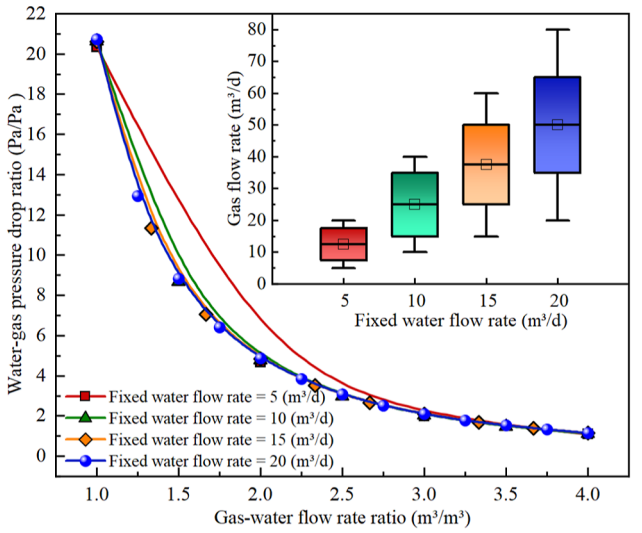

(a) Applicable gas flow rate range analysis when fixed different water flow rate

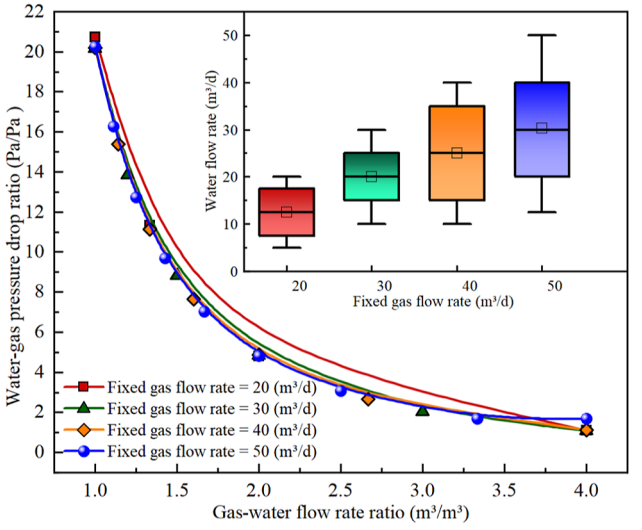

(b) Applicable water flow rate range analysis when fixed different gas flow rate

Figure 7. Analysis of the applicable flow range of the new AICD.

range of 5−20 m^3/d, within the range, when the water flow rate is 5 m^3/d, the water−gas pressure drop ratio is 1.083, and when the water flow rate increases to 20 m^3/d, the water−gas pressure drop ratio is 20.73, with the increase of the gas flow rate, when the gas flow rate is set at 50 m^3/d, the water flow rate increases to the range of 12.5−50 m^3/d. It can be concluded that if the tool is placed in a working environment where the water−gas pressure drop ratio is greater than or equal to 1, that is, the gas−water flow rate ratio is less than 4, the water control effect of the new AICD will be better exerted.

4.3. Experiment and Numerical Simulation Validation. In order to further verify the effectiveness of the new AICD for gas well water control and gas production, a single-phase experiment was conducted to verify the water control ability of the new AICD through indoor experiments, and the experimental results were compared to the simulation results. First, the new AICD was designed and manufactured, and the parameter values of the tool were consistent with those of the optimized simulation model; second, the experimental device was built; Figure 8 is the experimental flowchart diagram; the equipment in the experiment included a water tank, an oil tank, a gas compression tank, a positive displacement pump, a gas booster pump, flow meter, pressure transducers, AICD test article, and other components. Figure 8 shows the experimental flowchart diagram, in which the gas booster pump can compress air or nitrogen to the required pressure and store it in the gas compression tank; the pressure in the tank is kept constant through the pressure control valve, and a throttle valve is installed upstream of the AICD test article to adjust the gas flow rate and measure the gas flow rate through a flow meter; the gas is discharged into the atmosphere after passing through the AICD test article. The positive displacement pump can pump the water (or oil) in the circuit upstream of the AICD test article, and the upstream flow rate is measured by the flow meter and then flows through the AICD test article and returns to the storage tank. When the abovementioned gas, water (oil) passes through the upstream and downstream of the AICD test article, the pressure difference is transmitted to the paperless recorder by the

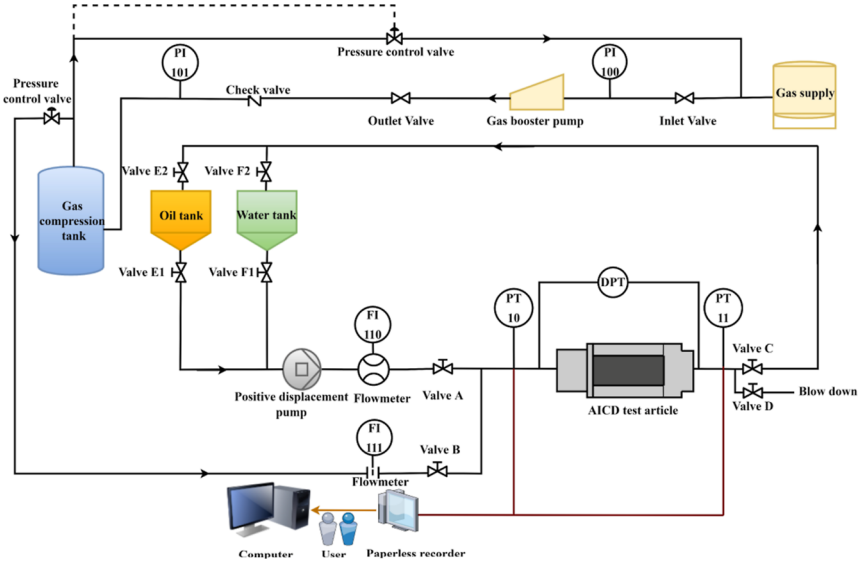

Figure 8. Experimental flowchart diagram.

https://doi.org/10.1021/acsomega.3c03807
ACS Omega 2023, 8, 39052−39066

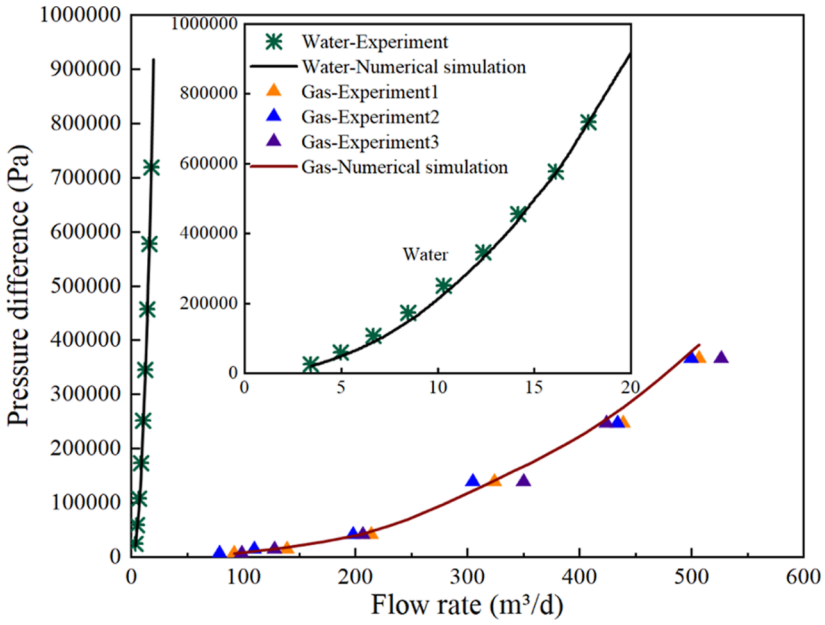

Figure 9. Comparison diagram of pressure drop data of single-phase flow test and numerical calculation.

pressure transducers and is observed and recorded by the experimenter.

The physical experiment is carried out on single-phase gas and water; the viscosity of water is 0.97 cP, the density is 993.5 kg/m^3, and the gas source used in the experiment is air. During the experimental process water test, the positive displacement pump can adjust the maximum frequency to 50 Hz, and the pumping water flow rate is 17.8 m^3/d, so the test flow range of water is set as (0−17.8 m^3/d); during the gas test, the test flow range of gas is set as (80−500 m^3/d). The numerical simulation sets the same gas flow rate value and water flow rate value as the experiment, the fluid parameters set water and air, in which the air can be compressed to a maximum density of 29 kg/m^3 according to the pressure of the gas compression tank of 2.5 MPa and the local experimental temperature, the actual operation and numerical simulation processes, adjust the gas compressor displacement, stabilize the density of compressed air in the gas compression tank to 15 kg/m^3, and other parameter settings are the same as the experimental conditions.

The paper compares the experimental results with the numerical simulation results through the error percentage, as shown in formula 14, the error percentage is the ratio of the absolute value of the difference between the experimental value and the simulated predicted value to the experimental value.[56] Figure 9 shows the comparison of experimental results with numerical results; the average error percentage between the experimental values of single-phase water and the numerical simulated values is 10.91%, which reveals relatively good agreement between the simulated and measured values; in addition, the pressure drop-flow rate relationship shows that, with the increase of the water flow rate, the pressure drop across the new AICD tends to increase gradually. However, when the experimental results and numerical results of single-phase gas are compared, there is a certain deviation between the experimental values and numerical calculation values, and the simulated values are greater than the experimental values. Because the flow of the gas after the throttle valve and before the inlet of the AICD test article fluctuates to a certain extent during the experiment, the maximum deviation is 26.01% and the minimum deviation is 1.70%. For this reason, multiple sets of experiments are carried out, and the readings are carried out when the pressure is relatively stable; they are, respectively, experiment 1, experiment 2, and experiment 3. Comparing the experimental results with the simulation results, the experimental results cannot be completely consistent with the numerical calculation results, but their general rules are consistent, with an average deviation of 11.85%, they all show that the pressure difference of the gas through the AICD test article gradually increases with the increase of the gas flow rate. Therefore, through experimental verification, the accuracy of the analysis of the water control ability of the new AICD can basically be judged, indicating that it has a good water control ability

$$\text{error percentage} = \frac{|\text{prediction} - \text{experimental value}|}{\text{experimental value}} 100 \quad (14)$$

5. CONCLUSIONS

In this paper, a novel AICD used for gas well water control and gas production is proposed, and then the DoE is performed to investigate the optimal structural parameters and the performance of the new AICD, finally carrying out the numerical simulation and indoor experiment under the same conditions. Also, the conclusions derived from this work can be summarized as follows.

(1) Through the DoE, the optimal structural parameters of the tool are determined: the angle of the Y-shaped channel is 60, the width of the q-shaped flow channel is 3, and the number of Y-shaped inlets and q-shaped flow channels are all 4. The rules of water and gas single-phase flow through the new AICD are studied by numerical simulation, the flow channel can be automatically identified according to the structure of the new AICD and the physical property difference of gas and water, and a small gas pressure drop and a large water pressure drop can be generated.

https://doi.org/10.1021/acsomega.3c03807
ACS Omega 2023, 8, 39052−39066

(2) The sensitivity analysis found that the density has a great influence on the pressure drop, while the viscosity has little impact on the pressure drop of the fluid. The flow rate range analysis shows that the gas−water flow rate ratio has a great influence on the water−gas pressure drop ratio; when the gas−water flow rate ratio is less than 4, the new AICD can exert its water control effect, and the smaller the gas−water flow rate ratio, the better the water control effect.

(3) The results of physical experiments are consistent with the simulation results; the average deviation of single-phase water is 10.91% and the average deviation of single-phase gas is 11.85%.

This work was carried out based on discovering shortcomings of the water management strategy of the drainage gas recovery technology in terms of the water control concept and proposing the gas well intelligent layered/segmented production and water control technology. The AICD used for water control and gas recovery in gas wells as its core component, to ensure that the gas flows smoothly inside it and to keep water under control to a greater extent, can maximize the performance of AICD tools, and the most important thing is that it can restrict the water in the formation from entering the wellbore, which can not only delay the premature entry of water into the wellbore but also shut-off the aquifer when the wellbore begins to accumulate fluid, prevent the impact of the water-producing layer/section on the entire gas well, and improve the gas recovery. However, the current research has not carried out the research on gas−water multiphase flow and has not carried out the relevant research on the gas well intelligent layered/segmented production and water control technologies based on the AWC optimization design. In future work, the performance of the new AICD and the optimization design of well completion can be improved from the perspectives of numerical simulation and theory.

AUTHOR INFORMATION

Corresponding Authors

Haitao Li − *State Key Laboratory of Oil & Gas Reservoir Geology and Exploitation, Southwest Petroleum University, Chengdu, Sichuan 610500, China*; Email: lihaitao@swpu.edu.cn

Hongwen Luo − *State Key Laboratory of Oil & Gas Reservoir Geology and Exploitation, Southwest Petroleum University, Chengdu, Sichuan 610500, China*; Email: rojielhw@163.com

Authors

Sujuan Gao − *State Key Laboratory of Oil & Gas Reservoir Geology and Exploitation, Southwest Petroleum University, Chengdu, Sichuan 610500, China*; orcid.org/0009-0000-9847-9360

Song Nie − *State Key Laboratory of Oil & Gas Reservoir Geology and Exploitation, Southwest Petroleum University, Chengdu, Sichuan 610500, China*

Ying Ai − *North China Oilfield Exploration and Development Research Institute, Renqiu 062552, China*

Ying Li − *State Key Laboratory of Oil & Gas Reservoir Geology and Exploitation, Southwest Petroleum University, Chengdu, Sichuan 610500, China*

Complete contact information is available at: https://pubs.acs.org/10.1021/acsomega.3c03807

Notes

The authors declare no competing financial interest.

ACKNOWLEDGMENTS

This study was funded by the China Postdoctoral Science Foundation (grant no. 2021M702721); Sichuan Natural Science Foundation (grant no. 2022NSFSC0993); and China Petroleum Science and Technology Innovation Fund Project (2022DQ02-0305). The authors would like to thank the State Key Laboratory of Oil and Gas Reservoir Geology and Exploitation, Southwest Petroleum University, for the technical support.

REFERENCES

(1) Ogolo, N. A.; Isebor, J. O.; Onyekonwu, M. O. Feasibility Study of Improved Gas Recovery by Water Influx Control in Water Drive Gas Reservoirs. *SPE*, 2014.

(2) Armenta, M.; Wojtanowicz, A. K. Severity of Water Coning in Gas Wells. *SPE*, 2002.

(3) Feng, X.; Zhong, B.; Yang, X.; Deng, H. Effective water influx control in gas reservoir development: Problems and countermeasures. *Nat. Gas Ind.* **2015**, *2*, 240−246.

(4) Tesha, J. M.; Qaseem, S.; Moreno, F. G.; Somerville, J. M. Predicting Performance of High Deliverability Horizontal Gas Wells and Control of Water Cresting in Tertiary Sands East Africa. *Int. J. Pertoleum and Pertochemical Eng.* **2019**, *5*, 17−51.

(5) Li, Q.; Yang, Y.; Peng, X. In Research on Water Intrusion Mechanism and Water Control Countermeasures of Water-Bearing Gas Reservoirs in Sichuan Basin. *2018 National Natural Gas Academic Annual Conference*; Fuzhou, Fujian, China, 2018; pp 28−37.

(6) Li, T. Characteristics of water influx in the development of the Puguang Gas Field, Sichuan Basin. *Nat. Gas. Ind.* **2014**, *34*, 65−71.

(7) Sech, R. P.; Jackson, M. D.; Hampson, G. J. In Controls on Water Cresting in High Productivity Horizontal Gas Wells. *SPE Europec/EAGE Annual Conference and Exhibition*; London, United Kingdom, 11−14 June; 2007.

(8) Qi, T.; Feng, J.; Xuan, Y.; He, J.; Shi, L. In Experimental Study on Combined Water Control Technology for High Temperature and High Pressure Deep Water Gas Reservoirs. *2022 International Conference on Cloud Computing, Big Data and Internet of Things (3CBIT)*; IEEE, 22−23 October; Wuhan, China, 2022; pp 293−296.

(9) Armenta, M. *Mechanisms and Control of Water Inflow to Wells in Gas Reservoirs with Bottom Water Drive*; Louisiana State University, 2003.

(10) Taha, A.; Amani, M. Overview of Water Shutoff Operations in Oil and Gas Wells; Chemical and Mechanical Solutions. *Chem. Eng.* **2019**, *3*, 51.

(11) Tugan, M. F. Deliquification techniques for conventional and unconventional gas wells: Review, field cases and lessons learned for mitigation of liquid loading. *J. Nat. Gas Sci. Eng.* **2020**, *83*, 103568.

(12) Wang, D.; Li, Y.; Ma, L.; Yu, F.; Liu, S.; Qi, T.; Jiang, S. Evaluation of the Effectiveness and Adaptability of a Composite Water Control Process for Horizontal Wells in Deepwater Gas Reservoirs. *Front. Earth Sci.* **2022**, *10*, 906949.

(13) Shaffee, A.; Ghazali, H.; Rajan, P.; Mohamad, W.; Thant, M.; Bakar, M. In *Extending the Performance of Standalone Sand Screens (SAS) with Flow Segmentizers in Gas Wells*; ADIPEC, Abu Dhabi, UAE, 31 October−3 November, 2022.

(14) Nie, S.; Li, H.; Luo, H.; Gao, S.; Ma, X.; Wang, L.; Wang, X. A new method for designing parameters of sand control gravel based on particle discrete elementmethod. *Sci. Technol. Eng.* **2023**, *23* (08), 3237−3243.

(15) Nie, S.; Li, H.; Gao, S.; Hu, Z.; Luo, H.; Li, Q.; Ma, X.; Cui, X.; Liu, Z.; Zhang, L. Numerical simulation and experimental study on the whole process of gravel packing in horizontal wells. *Geoenergy Sci. Eng.* **2023**, *224*, 211603.

(16) Al-khelaiwi, F.; Davies, D. In Advanced Sand-Face Completion Design and Application in Gas and Gas-Condensate Fields. *Society of Petroleum Engineers - SPE Asia Pacific Oil and Gas Conference and Exhibition 2010*; APOGCE 2010, 2010.
(17) Al-Khelaiwi, F. T. *A Comprehensive Approach to the Design of Advanced Well Completions*; Philosophy, Heriot-Watt University, 2013.
(18) Cui, X.; Li, H.; Li, S.; Cai, B.; Li, Y.; Ge, J.; Wang, N. Integrated intelligent well completion technology of water detection and water control in horizontal well and its application. *China Offshore Oil Gas* **2021**, *33* (05), 158−164.
(19) Zuo, K.; Yang, J.; Luo, H.; Li, H.; Xiang, Y.; Li, Y.; Jiang, B.; Nie, S.; Zhang, Q. An efficient inversion method to interpret distributed temperature measurement of horizontal wells in shale gas reservoirs. *Pet. Sci. Technol.* **2023**, 1−22.
(20) Hansong, M.; Luo, H.; Haitao, L.; Yuxing, X.; Qin, Z.; Ying, L. Study on the Influence Law of Temperature Profile of Vertical Wells in Gas Reservoirs. *Int. J. Petrol. Sci. Technol.* **2022**, *9*, 54−66.
(21) Luo, H.; Xiang, Y.; Li, H.; Tan, Y.; Pang, W.; Zhang, Q.; Ma, X.; Liu, C. An efficient inversion interpretation method for distributed temperature measurement of horizontal wells in shale gas reservoirs. *J. Univ. Pet., China (Ed. Nat. Sci.)* **2023**, *47* (03), 115−121.
(22) Luo, H.; Li, Y.; Li, H.; Cui, X.; Chen, Z. Simulated Annealing Algorithm-Based Inversion Model To Interpret Flow Rate Profiles and Fracture Parameters for Horizontal Wells in Unconventional Gas Reservoirs. *SPE J.* **2021**, *26* (04), 1679−1699.
(23) Al-Khelaiwi, F. T.; Davies, D. R. In Advanced Sand-Face Completion Design and Application in Gas and Gas-Condensate Fields. *SPE Asia Pacific Oil and Gas Conference and Exhibition*; Brisbane, Queensland, Australia, 18−20 October; 2010.
(24) Shi, W.-p.; Zhao, X.; Hu, X.-j.; Yu, T.-m.; Liu, B.-w.; Duan, Y. Design and numerical simulation of water restriction device AICD for natural gas exploitation. *J. Jilin Univ. (Eng. Technol. Ed.)* **2019**, *49* (06), 1986−1991.
(25) Zhao, Y. Structural design and numerical simulation of underground water control device. Master Thesis; Jilin University, 2020.
(26) Zhou, C.; Zhao, X.; Yao, Z.; Dang, S.; Kou, X. Optimization of AICD well completion technology in horizontal wells in gas reservoirs with bottom water. *Xinjiang Pet. Geol.* **2020**, *41* (04), 444−449.
(27) Hong, K. C. Two-Phase Flow Splitting at a Pipe Tee. *J. Petrol. Technol.* **1978**, *30* (02), 290−296.
(28) Oranje, L. Condensate Behavior in Gas Pipelines is Predicable. *Oil Gas J.* **1973**, *71* (27), 39−44.
(29) Thorn, R.; Johansen, G. A.; Hammer, E. A. Recent developments in three-phase flow measurement. *Meas. Sci. Technol.* **1997**, *8* (7), 691−701.
(30) Lin, Z. Characteristics of gas-liquid two-phase flow in pipelines and their engineering applications. Xi'an Jiaotong University Press: Xi'an, 1992.
(31) Wang, D.; Zhang, X.; Lin, Y.; Lin, Z. The split of two-phase flow at horizontal T-junctions of unequal diameters. *J. Eng. Thermophys.* **2003**, *2*, 259−261.
(32) Azzopardi, B. J.; Rea, S. N. Phase separation using a simple T-junction, *SPE Annual Technical Conference and Exhibition*; 2000.
(33) He, K.; Wang, S.; Huang, J. The effect of flow pattern on split of two-phase flow through a micro-T-junction. *Int. J. Heat Mass Transfer* **2011**, *54* (15−16), 3587−3593.
(34) Zhang, N.; Li, H.; Zhang, Y.; Deng, Q.; Tan, Y. A Numerical Simulation for the Determination of the Shunt Ratio at a T-Junction With Different Branch Angles, Viscosities, and Flow Rates. *J. Energy Resour. Technol.* **2019**, *141* (10), 102906.
(35) Fripp, M.; Zhao, L.; Least, B. The Theory of a Fluidic Diode Autonomous Inflow Control Device. *SPE Middle East Intelligent Energy Conference and Exhibition*, 2013.
(36) Least, B.; Greci, S.; Burkey, R.; Ufford, A.; Wileman, A. Autonomous ICD Single Phase Testing. *SPE Annual Technical Conference and Exhibition*, 2012.
(37) Least, B.; Greci, S.; Wileman, A.; Ufford, A. Fluidic Diode Autonomous Inflow Control Device Range 3B - Oil, Water, and Gas Flow Performance Testing. *SPE Kuwait Oil and Gas Show and Conference*, 2013.
(38) Zhao, L.; Least, B.; Greci, S.; Wileman, A. Fluidic Diode Autonomous ICD Range 2A Single-Phase Testing. *SPE Oilfield Water Management Conference and Exhibition*, 2014.
(39) Least, B.; Greci, S.; Wileman, A.; Ufford, A. Autonomous ICD Range 3B Single-Phase Testing. *SPE Annual Technical Conference and Exhibition*, 2013.
(40) Corona, G.; Greci, S.; Least, B.; Yin, W.; Plumlee, J. Fluidic Diode Autonomous ICD Single-Phase Testing. *SPE Deepwater Drilling and Completions Conference*, 2016.
(41) Least, B.; Bonner, A.; Regulacion, R.; Peñaranda, R.; Sampedro, T.; Coloma, F. Autonomous ICD Installation Success in Ecuador Heavy Oil: A Case Study. *SPE Annual Technical Conference and Exhibition*, 2013.
(42) Shahreyar, N.; Corona, G.; Miller, B. Multilateral Well Construction with Fluidic Diode AICD Completion Technologies: Case Study, North West Shelf, Western Australia. *Offshore Technology Conference Asia*, 2020.
(43) Kalyani, T.; Corona, G.; Ross, K. Fluidic Diode Autonomous ICD Selection Criteria, Design Methodology, and Performance Analysis for Multiple Completion Designs: Case Studies. *SPE Conference at Oman Petroleum & Energy Show*, 2022.
(44) Corona, G.; Fripp, M.; Kalyani, T.; Yin, W. Fluidic Diode Autonomous Inflow Control Device for Heavy Oil Application. *SPE Heavy Oil Conference and Exhibition*, 2016.
(45) Corona, G.; Fripp, M.; Yin, W. Fluidic Diode Autonomous ICD Multiphase Performance in Light-Oil Reservoirs. *SPE Middle East Oil & Gas Show and Conference*; 2017.
(46) Zeng, Q.; Wang, Z.; Wang, X.; Wei, J.; Zou, L.; Li, Y. A new type design of AICD and its numerical simulation. *Oil Drill. Prod. Technol.* **2015**, *37* (02), 101−106.
(47) Zeng, Q.; Wang, Z.; Wang, X.; Wei, J.; Zhang, Q.; Yang, G. A novel autonomous inflow control device design and its performance prediction. *J. Petrol. Sci. Eng.* **2015**, *126*, 35−47.
(48) Yang, M.; Li, H.; Xie, J.; Wang, Y.; Jiang, R.; Zhu, S.; Li, Y. The theory of the automatic phase selection controller and its performance analysis. *J. Pet. Sci. Eng.* **2016**, *144*, 28−38.
(49) Li, H.; Liu, Q.; Wang, N.; Zhang, N.; Cui, X. R&D of a new autonomous inflow control device for horizontal wells and fluid sensitivity analysis. *China Offshore Oil Gas* **2019**, *31* (01), 126−132.
(50) Cui, X.; Li, Y.; Li, H.; Luo, H.; Zhang, J.; Liu, Q. A Novel Automatic Inflow-Regulating Valve for Water Control in Horizontal Wells. *ACS Omega* **2020**, *5* (43), 28056−28072.
(51) Sultan, R. A.; Rahman, M. A.; Rushd, S.; Zendehboudi, S.; Kelessidis, V. C. Validation of CFD model of multiphase flow through pipeline and annular geometries. *Part. Sci. Technol.* **2019**, *37*, 685−697.
(52) Launder, B. E.; Spalding, D. B. *Lectures in Mathematical Models of Turbulence*; Academic Press: London, 1972.
(53) Kang, Z.; Xie, K. S-K equations of calculating formatiom water density. *Sci. Technol. Eng.* **2012**, *12* (01), 19−24.
(54) Schowalter, T. T. Mechanics of Secondary Hydrocarbon Migration and Entrapment. *AAPG Bull.* **1979**, *63*, 723−760.
(55) Fu, X.; Wang, Z.; Zhu, X. Study on the density of the formation water under different temperature and salinity. *J. Daqing Pet. Inst.* **1998**, *2*, 8.
(56) Huque, M. M.; Butt, S. D.; Zendehboudi, S.; Imtiaz, S. A. Systematic sensitivity analysis of cuttings transport in drilling operation using computational fluid dynamics approach. *J. Nat. Gas Sci. Eng.* **2020**, *81*, 103386.

https://doi.org/10.1021/acsomega.3c03807
ACS Omega 2023, 8, 39052−39066